Catalysis Science & Technology

Accepted Manuscript

ROYAL SOCIETY OF CHEMISTRY

www.rsc.org/catalysis

Theoretical Investigation of the Hydrodeoxygenation of Methyl Propionate over Pd (111) Model Surfaces

Sina Behtash, Jianmin Lu, and Andreas Heyden *

Department of Chemical Engineering, University of South Carolina, 301 S. Main St., Columbia, South Carolina 29208, USA

* Corresponding author, Email: heyden@cec.sc.edu

Abstract

Esters are one of the key components of lipid-rich biomass feedstocks that are potential raw materials for production of green fuels. We present a thorough density functional theory and microkinetic modeling study of the hydrodeoxygenation (HDO) of organic esters over Pd (111) model surfaces. Methyl propionate was chosen as our model molecule since it permits the study of the effect of both α- and β-carbon dehydrogenations on the HDO of esters while still being computationally accessible. An extensive network of elementary reactions was investigated and a microkinetic model was developed at reaction conditions of 473K, a methyl propionate partial pressure of 0.01 bar, and a hydrogen partial pressure of 0.2 bar to identify the dominant pathway and abundant surface species. Our microkinetic model suggests that decarbonylation pathways of methyl propionate are favored over decarboxylation pathways. We found the most dominant pathway to involve methyl propionate to undergo two dehydrogenation steps of both α- and β-carbons to form $CH_2CHCOOCH_3$, followed by C-O and C-C cleavages to produce C2 hydrocarbons and methoxy that eventually get hydrogenated to ethane and methanol ($CH_3CH_2COOCH_3 \rightarrow CH_3CHCOOCH_3 \rightarrow CH_2CHCOOCH_3 \rightarrow CH_2CHCO+OCH_3$ $\rightarrow \ldots \rightarrow CH_3CH_3+CO+CH_3OH$). The most abundant surface intermediates were identified to be H and CO and CH_3C. Finally, a sensitivity analysis of our models suggests that the dehydrogenation of the α-carbon of methyl propionate, as well as propanoyl-methoxy bond dissociation control the overall rate on Pd (111).

Keywords: biomass; lipids; triglyceride; ester; methyl propionate; palladium; density functional theory; hydrodeoxygenation; decarbonylation; decarboxylation;

1. Introduction

Energy demand continues to significantly increase due to societal developments. As a result, fossil fuels have been overused and nowadays most countries are strongly dependent on fossil fuel imports.[1,2] Rising concerns over depletion of current fossil fuel resources and also environmental impacts of fossil fuel utilization have drawn substantial attention to conversion of biomass to biofuels to at least partially meet the world's growing energy demand. First generation biofuels such as bio-ethanol and biodiesel have been implemented successfully in the energy system. However, they generally suffer from compatibility issues and low energy density.[3-6] Recently, biofuels research has been focused on the development of the science and technology for conversion of biomass into second-generation biofuels that are identical to gasoline and diesel and which are often called green diesel or green gasoline.[7]

Lipid-rich biomass feedstocks such as vegetable oils are one potential raw material for production of green fuels. In spite of their current relatively high price,[8] it is expected that the availability of lipid feedstocks will increase in the near future due to recent progress in large-scale production of non-edible lipid-rich biomass such as algae,[9-11] Jatropha and Camelina oils.[12-14] Lipids contain considerable amounts of oxygenates such as triglycerides/organic esters and fatty acid. To convert the lipids into hydrocarbons identical to fossil-derived transportation fuels, removal of oxygen atoms from the feedstock molecules is required. Significant research efforts have been done to convert vegetable oils into liquid hydrocarbons employing a hydroprocess with conventional hydrotreating catalysts such as sulfided $NiMo/Al_2O_3$ and $CoMo/Al_2O_3$.[15-17] However, by using conventional, sulfided hydrotreating catalysts, the sulfur content of the final products is remarkable. Additionally, other disadvantages such as short catalyst life time and problems in separation of carbon oxides from the recycle gas have been reported.[15,17]

Consequently, there is an apparent need for new hydrodeoxygenation (HDO) catalysts for triglycerides/organic esters and fatty acids.

To rationally design a metal catalyst for hydrotreating of lipids, it is necessary to obtain a fundamental understanding of the reaction mechanisms on the catalyst surface. Previously, various reaction routes such as decarbonylation (DCN), decarboxylation (DCX), and reductive deoxygenation (RDO) have been proposed for the catalytic hydrodeoxygenation (HDO) of triglycerides to alkanes.[15] There is a consensus that RDO is not the dominant reaction mechanism over most metal catalysts;[15,18,19] however, it is currently not clear whether DCX or DCN are the dominant pathways. A thorough theoretical investigation of the catalytic HDO of fatty acids and esters can provide the required knowledge about the activity of the oxygen functionality in organic acids and esters. Also, the results of such studies can be used for the design of new metal catalysts for upgrading wood-derived bio-oils that contain considerable amounts of acids and esters.[20] In our recent publications,[21,22] we investigated the HDO of organic acids in the absence and presence of solvents. In this study, we focused on understanding the reaction mechanism for the catalytic HDO of organic esters under gas phase condition with the help of first principles calculations. Previously, the activation of esters over various metal catalysts has been investigated by a number of research groups. For example, Murzin et al. investigated the HDO of ethyl stearate over Pd/C catalysts in a detailed experimental study.[18] Their observations suggested that the reaction mechanism is complex and the DCN is the dominant catalytic cycle in the presence of hydrogen while DCX is favored in the absence of hydrogen. Similar results have been obtained in a study[19] of methyl stearate and methyl octanoate over Pd/Al_2O_3. Next, the catalytic conversion of methyl acetate to alcohols over palladium was theoretically investigated by Xu et al.[23] They reported that the activation of

methyl acetate over Pd (111) is limited by the dehydrogenation of the alpha, beta and methoxy carbons. Dehydrogenation from the methoxy end leads to a selective C-O dissociation to produce methoxy and acetaldehyde; however, dehydrogenation of the alpha and beta carbon was shown to be an unselective pathway, i.e., further activation of the dehydrogenated species could not be determined without a detailed microkinetic modeling analysis.

In this paper, we present a thorough density functional theory (DFT) and microkinetic modeling study of the HDO of organic esters over Pd (111) model surfaces. Methyl Propionate was purposefully chosen as our model molecule. Methyl Propionate is the smallest organic ester that has two carbon atoms (alpha and beta carbons) next to the carbonyl function that allows us to investigate whether dehydrogenation of alpha and beta carbons can affect C-O and C-C bond dissociations and overall activity. All possible C-C, C-O and dehydrogenation/hydrogenation steps for methyl propionate and derivatives have been investigated in detail to obtain an extensive chemical reaction network. Next, the results of the DFT calculations were used to obtain reaction rate parameters such as elementary reaction rate constants. Finally, these parameters were incorporated in a microkinetic model to obtain the overall turnover frequency, dominant reaction pathway, and most abundant species on the surface.

2. Methods

2.1 DFT Calculations

All density functional theory calculations have been conducted using the Vienna Ab Initio Simulation Package (VASP).[24-26] The Kohn-Sham valence states are expanded in a plane wave basis sets with the energy cut-off of up to 400eV. The interaction between core electrons is described with projector-augmented wave (PAW)[25,27] methods. The exchange correlation energy

is calculated within the generalized gradient approximation (GGA) using the functional form proposed by Perdew and Wang which is known as Perdew-Wang 91 (PW91).[28,29] We note that the PW91 functional does not contain any dispersion interactions. As a result, adsorption energies of hydrocarbon molecules computed with PW91 are possibly underestimated. Considering though that the PW91 functional generally overestimates adsorption energies[30]and that surface reaction energies computed with the PW91 and PBE-D3 functionals (a functional that contains an empirical corrections for dispersion interactions[31]) are within the error of DFT (± 0.2 eV), PW91 calculations will likely lead to reasonable reaction energies. The lattice constant, obtained from the optimization of the fcc-Pd bulk, is 3.953 $\AA$ which is in reasonable agreement with the experimental value of 3.891 $\AA$. The surface Brillouin zone is sampled with $4\times4\times1$ Monkhorst-pack kpoint grid. Pd (111) is modeled by a four layer slab with a (3×4) surface unit cell and the palladium layers separated by a 15 $\AA$ vacuum. The 12 Pd atoms in each layer allow for a coverage of 1/12 ML for adsorbates. The bottom two Pd layers were fixed to their bulk configuration during all calculations while top two layers were free to relax in all directions. Adsorption energies of all intermediates were calculated at their most stable geometry by the following equation:

$$E_{\text{ads}} = E_{\text{slab+adsorbate}} - E_{\text{slab}} - E_{\text{adsorbate(gas)}} \quad (1)$$

where $E_{\text{slab+adsorbate}}$ is the total energy of the adsorbed intermediate on the Pd slab, E_{slab} is the total energy of the Pd slab and $E_{\text{adsorbate(gas)}}$ is the total energy of the adsorbate in the gas phase. Transition states are located by combination of CI-NEB[32] and dimer[33,34] methods and finally, vibrational frequency calculations have been performed to clearly identify stable intermediate and transition state structures. The zero-point energy correction for all the structures was taken into account by using the following equation:

$$\Delta E_{ZPE} = \sum_i \frac{1}{2} h \nu_i \quad (2)$$

where h is the Plank constant and ν_i is the vibrational frequency of mode i. We note that all the energy values in this paper are zero-point energy corrected.

2.2 Microkinetic modeling

For surface reactions, the forward rate constant (k_{for}) of each reaction is calculated using harmonic transition state theory (hTST)[35]

$$k_{for} = \frac{k_B T}{h} \frac{q_{TS,vib}}{q_{IS,vib}} e^{-\frac{E_{a\_for}}{k_B T}} \quad (3)$$

where k_B is the Boltzmann constant, T denotes the reaction temperature, h is the Planck constant, E_{a_for} stands for the zero-point energy-corrected activation barrier for the forward reaction derived from DFT calculations, and $q_{TS,vib}$ and $q_{IS,vib}$ are the (harmonic) vibrational partition functions for the transition state and the initial state, respectively, i.e., q_{vib} is calculated as

$$q_{vib} = \prod_i \frac{1}{1 - e^{\frac{-h\nu_i}{k_B T}}} \quad (4)$$

where ν_i is the vibrational frequency of each vibrational mode of the adsorbed intermediate derived from our DFT calculations.

The reverse rate constant (k_{rev}) is calculated similarly and the thermodynamic equilibrium constant K is given as

$$K = \frac{k_{for}}{k_{rev}} \quad (5)$$

For an adsorption reaction A(g)+*→A*, the equilibrium constant K is defined as

$$K = \frac{(q_{vib})_{A*}}{(q_{vib} q_{rot} q_{trans})_{A(g)}} e^{\frac{-\Delta E_{ads}}{k_B T}} \quad (6)$$

where $(q_{vib})_{A*}$ is the vibrational partition function of adsorbed A, and q_{vib}, q_{rot}, q_{trans} stand for vibrational, rotational, and translational partition functions, respectively. ΔE_{ads} represents the zero-point corrected adsorption energy. For an adsorption reaction A(g)+*→A*, the forward rate is given by collision theory with a sticking probability of 1.

$$k_{for} = \frac{1}{N_0\sqrt{2\pi m_A k_B T}} \quad (7)$$

where N_0 is the number of sites per area (1.478×10^{19} m^2) and m_A denotes the molecular weight of A. The reverse rate constant is again given as

$$k_{rev} = \frac{k_{for}}{K} \quad (8)$$

With the forward and reverse rate constants defined, we solve the full set of steady-state rate equations to obtain the surface coverages of all possible reaction intermediates and the fraction of free sites using the BzzMath library[36] developed by Buzzi-Ferraris. No assumptions were made regarding rate-limiting steps.

3. Results

3.1 Adsorption and Desorption Reactions

Methyl propionate (MP) adsorbs weakly on Pd (111) (E_{ads}=-0.52 eV). In the most stable *cis* configuration of adsorbed methyl propionate the carbonyl oxygen binds to a single Pd atom (atop-site) with the molecular plane perpendicular to the surface (Figure 1.1). In the *trans* configuration (Figure1.2), the two oxygen atoms of methyl propionate are located above a pair of adjacent Pd atoms (bridge-site) with an zero-point corrected adsorption energy of E_{ads}=-0.50 eV. Another possible configuration is the *chair* configuration, (Figure 1.3) in which the two oxygen atoms and the carbonyl carbon atom bind to three palladium atoms (E_{ads}=-0.50 eV). The weak π-

bonded interactions of the C=O group with the surface[37] explains the quite small adsorption energy of MP (the three adsorption configurations of MP and all intermediates involved in the hydrodeoxygenation of MP are shown in Figure 1).

We will later show in our microkinetic analysis (Section 4.1), that we identified methanol, CO, ethane and ethene to be the main products of HDO of methyl propionate over Pd (111) model surfaces. Methanol adsorbs weakly on Pd (111) with zero-point corrected adsorption energy of -0.32 eV. In the adsorption configuration, the oxygen atom binds to one Pd atom (atop site). Ethane also physisorbs on palladium and adsorption energy of this intermediate is -0.17 eV. However, ethene and CO adsorb stronger with adsorption energies of -0.98 and -1.97 eV respectively. Additionally, the H_2 that was fed to the reactor with methyl propionate adsorbs dissociatively with an adsorption energy of -1.13 eV. Finally we note that the reaction parameters for all of the adsorption and desorption reactions, as well as their correspondent rate constants that were used in our microkinetic model, are presented in Table 1 and 2 (Step 65-73).

(Figure 1 Here)

(Table 1 Here)

3.2 Elementary Surface Reactions

The investigated elementary reactions in the HDO of methyl propionate can be grouped into three different types of bond dissociations: C-O bond dissociations (e.g. $CH_3CH_2COOCH_3 \rightarrow CH_3CH_2CO + OCH_3$), C-H bond dissociations (e.g. $CH_3CH_2COOCH_3 \rightarrow CH_3CHCOOCH_3$), and C-C bond dissociations (e.g. $CH_3CH_2CO \rightarrow CH_3CH_2 + CO$). The Zero-point corrected DFT-derived reaction energies, activation barriers, transition

state (TS) imaginary frequencies, and TS bond lengths for all types of the elementary reactions investigated in HDO of methyl propionate, are listed in Table 1. Additionally, a schematic of the transition state geometry configurations are illustrated in Figure 2.

(Figure 2 Here)

C-O bond dissociations:

Adsorbed methyl propionate can go through two different C-O bond dissociations to either form propionate and methyl (Step 1: $CH_3CH_2COOCH_3$** + 1* ↔ CH_3CH_2COO** + CH_3*) or propanoyl and methoxy (Step 2: $CH_3CH_2COOCH_3$** + 2*↔ CH_3CH_2CO*** + CH_3O*). Our DFT result suggests that the propanoyl-methoxy bond is easier to cleave as the activation barrier of this step ($E_{act\text{-}step2}$= 0.73 eV) is remarkably smaller than the activation barrier of the methyl-propionate bond dissociation ($E_{act\text{-}step1}$= 1.54 eV). The trend in the activation barriers stays the same for other dehydrogenated derivatives of methyl propionate, such as $CH_3CHCOOCH_3$, $CH_2CH_2COOCH_3$, $CH_2CH_2COOCH_3$, and $CH_2CHCOOCH_3$ (Table 1). Consequently, propanoyl-methoxy type C-O bond dissociations are expected to be more favored in comparison to propionate-methyl type C-O bond dissociations.

Next, propanoyl (CH_3CH_2CO) goes through dehydrogenation and C-C bond cleavages to produce CO, and is one of the key intermediates in the decarbonylation (DCN) mechanism, while propionate undergoes dehydrogenation and C-C dissociation steps to produce CO_2 and is essential to decarboxylation (DCX) reactions. Considering that production of propanoyl from methyl propionate and its dehydrogenated intermediates is more favored than production of

propionate, we predict the DCN to be the dominant mechanism. In section 4.1, we verified our prediction by a microkinetic modeling analysis under realistic reaction conditions.

C-H bond dissociations:

Adsorbed methyl propionate can be dehydrogenated via its α-, β-, and methoxy-end carbon. The dehydrogenation of the α-carbon (Step 3: $CH_3CH_2COOCH_3$** + 2* ↔ $CH_3CHCOOCH_3$*** + H*) is slightly exothermic (ΔE_0= -0.07 eV) and the activation barrier for this reaction is relatively small (0.70 eV). Dehydrogenation of the β-carbon (Step 4: $CH_3CH_2COOCH_3$** + 2* ↔ $CH_2CH_2COOCH_3$*** + H*) is slightly endothermic (ΔE_0=0.12 eV) and the activation barrier of this step is 0.78 eV. Finally, dehydrogenation of the methoxy-end carbon (Step 5: $CH_3CH_2COOCH_3$** + 2* ↔ $CH_3CH_2COOCH_2$*** + H*) is an almost thermoneutral process (ΔE_0=0.02 eV) with an activation barrier of 0.72 eV. We found that all dehydrogenations of α-, β-, and methoxy-end carbon have similarly small activation barriers and consequently, it is not possible to determine the dominant dehydrogenation pathway without developing a microkinetic model. However, all of these steps are less endothermic than the propanoyl-methoxy dissociation (ΔE_0=0.19) and consequently, we expect the dehydrogenation of methyl propionate to be slightly more favored than the propanoyl-methoxy dissociation.

The dehydrogenated derivatives of methyl propionate, $CH_3CHCOOCH_3$, $CH_2CH_2COOCH_3$, and $CH_3CH_2COOCH_2$, can go through C-O bond dissociations or further dehydrogenation steps. All possible elementary reactions for these intermediates are identified and the reaction parameters of these elementary steps are listed in Table 1. Our DFT results (as well as our microkinetic modeling analysis in section 4.1) suggest that both $CH_2CH_2COOCH_3$ and $CH_3CHCOOCH_3$ go through further dehydrogenation to form $CH_2CHCOOCH_3$, as Step 8

($CH_3CHCOOCH_3$*** + 1* ↔ $CH_2CHCOOCH_3$*** + H*, ΔE_0= -0.47 eV and E_{act}=0.46 eV), and Step 18 ($CH_2CH_2COOCH_3$*** + 1* ↔ $CH_2CHCOOCH_3$*** + H*, ΔE_0= -0.67 eV and E_{act}=0.34 eV) are exothermic and have very small activation barriers. We again considered various possible elementary reactions for further activation of $CH_2CHCOOCH_3$, but we will show below that these intermediates will go through C-O bond dissociation to form methoxy and CH_2CHCO where it next goes through C-C bond dissociation to form CH_2CH and CO.

In contrast to $CH_2CH_2COOCH_3$ and $CH_3CHCOOCH_3$, we predict that $CH_3CH_2COOCH_2$ undergoes a C-O bond dissociation to form propanoyl and OCH_2 (Step 28: $CH_3CH_2COOCH_2$*** + 3* ↔ CH_3CH_2CO*** + OCH_2***) since this step is exothermic by -0.31 eV and has a small activation barrier of 0.15 eV.

C-C bond dissociations:

Propanoyl (CH_3CH_2CO) and other dehydrogenated derivatives of propanoyl, such as CH_3CHCO, CH_3CCO, CH_2CHCO, and CHCHCO can go through C-C bond dissociations to produce C_2 fragments and CO on the surface (Step30, 32, 34, 36, and 37). Dissociation of the C-C bond in propanoyl (Step 30) is exothermic, ΔE_0= -0.60, but this step has a large activation barrier of 1.01 eV. Dehydrogenation of the α- and β- carbon of propanoyl facilitate the C-C bond dissociation. For instance the dissociation of the C-C bond of CH_3CCO (Step 37: CH_3CCO*** ↔ CH_3C* + CO* + 1*) has an activation barrier of 0.44 eV. So it is expected that propanoyl will go through further dehydrogenation steps of the α- and β- carbons prior to C-C bond cleavages. In the investigated reaction network of the HDO of methyl propionate we included various C-C bond dissociations, e.g., the decomposition of methyl propionate to CH_3CH_2 and $COOCH_3$ (NEB calculations predict an activation barrier of 2.07 eV), and propionate decomposition to CH_3CH_2

and CO_2 (Step 61, E_a=1.22 eV); however, as we explained before, our DFT results indicate that it is not probable that other C-C bond cleavages play an important role in the HDO of methyl propionate.

4. Discussions

4.1 Microkinetic Modeling

We previously[38] developed mean-field microkinetic models for the reaction mechanism of the decarboxylation and decarbonylation of propionic acid over Pd (111) model surfaces under realistic experimental gas phase conditions. In this study, we used the same methodology for developing a microkinetic model for the HDO of methyl propionate. All calculations were carried out at 473 K and partial pressures of methyl propionate and hydrogen of 0.01 and 0.2 bar, respectively, which are typical experimental conditions.[18,39-45] Since we did not include a water-gas shift model in our microkintic model, we had to set the partial pressures of CO and CO_2 to 0.001 bar which correspondents to approximately 10% conversion. Computed turnover frequencies (TOF) of all elementary steps are summarized in Table 2.

(Table 2 Here)

The most abundant surface intermediates were adsorbed hydrogen, CO, and CH_3C with surface coverages of 67%, 20%, and 7% respectively. The free site coverage is 6%. We note that we used a method similar to Grabow *et al.*[46] for determining coverage dependent adsorption energies of CO, H, and CH_3C. More details about adsorbate-adsorbate interactions can be found in our previously published paper.[38] A schematic of the most dominant reaction pathways is illustrated in Figure 3. The overall TOF is calculated to be 3.42×10^{-7} s^{-1} on Pd (111). As shown

in Figure 3, the adsorbed methyl propionate molecule can be dehydrogenated from the α, β or methoxy-end (Step 3, 4, and 5 respectively) or it can go through propanoyl-methoxy bond dissociations (Step 2). Accordingly, there are four competing pathways and this study can only suggest that the most dominant pathway might involve methyl propionate to undergo two dehydrogenation steps of first α- and then β-carbon to form $CH_2CHCOOCH_3$ followed by C-O bond dissociation to form CH_2CHCO and OCH_3. CH_2CHCO goes through C-C bond cleavage to produce C2 hydrocarbons (Step 34) while the methoxy group gets hydrogenated to form methanol (Step 57). The TOF of methanol formation (Step 57: $CH_3O + H \rightarrow CH_3OH$) is $TOF_{Step57}=2.47\times10^{-7}$ s^{-1}, which is one order of magnitude larger than the competing dehydrogenation of methoxy to formaldehyde (Step 54: $CH_3O \rightarrow CH_2O + H$, $TOF_{Step57}=1.45\times10^{-8}$ s^{-1}). According to our DFT results (Table 1), formation of methanol from methoxy (Step 57) and decomposition of methoxy to CO (Step 54-56) are thermodynamically competitive; however, our microkinetic modeling result shows that methanol formation is favored due to an excess of hydrogen on the surface (dominant pathway: $CH_3CH_2COOCH_3 \rightarrow CH_3CHCOOCH_3 \rightarrow CH_2CHCOOCH_3 \rightarrow CH_2CHCO+OCH_3 \rightarrow \ldots \rightarrow CH_3CH_3+CO+CH_3OH$, $TOF=1.85\times10^{-7}$ s^{-1}, red pathway in Figure 3).

In the second competitive pathway, methyl propionate gets dehydrogenated at the methoxy end to form $CH_3CH_2COOCH_2$ followed by C-O bond dissociation to form propanoyl (CH_3CH_2CO) and formaldehyde. Next, propanoyl gets dehydrogenated prior to C-C bond cleavage to form C_2 hydrocarbons and CO. Formaldehyde again can be further dehydrogenated to produce CO ($CH_3CH_2COOCH_3 \rightarrow CH_3CH_2COOCH_2 \rightarrow CH_3CH_2CO+OCH_2 \rightarrow \ldots \rightarrow CH_3CH_3+2CO$, green pathway in Figure 3). The computed TOF of the dominant pathway is only 2.4 times larger than for this pathway.

In the third pathway, methyl propionate directly dissociates to form methoxy and propanoyl ($CH_3CH_2COOCH_3 \rightarrow CH_3CH_2CO \rightarrow \ldots \rightarrow CH_3CH_3+CO+CH_3OH$, TOF=$6.43\times10^{-8}$ s^{-1}, black pathway in Figure 3). Later, the methoxy group gets hydrogenated to form methanol and the propanoyl species gets dehydrogenated followed by C-C bond cleavage to produce C2 hydrocarbons and CO.

In the last competitive pathway, methyl propionate first undergoes a dehydrogenation via its β-carbon, followed by another dehydrogenation from its α-carbon to produce $CH_2CHCOOCH_3$. This intermediate goes through C-O bond dissociation to form CH_2CHCO and methoxy. We note that the only difference of this pathway and the most dominant pathway is in the order of dehydrogenation steps. In the dominant pathway, first α-carbon and then β-carbon gets dehydrogenated while in this pathway first the β-carbon and then the α-carbon get dehydrogenated. However, it is less probable that methyl propionate first goes through dehydrogenation of the β-carbon as the TOF of this pathway is an order of magnitude smaller than the most dominant pathway ($CH_3CH_2COOCH_3 \rightarrow CH_2CH_2COOCH_3 \rightarrow CH_2CHCOOCH_3 \rightarrow CH_2CHCO+OCH_3 \rightarrow \ldots \rightarrow CH_3CH_3+CO+CH_3OH$, TOF=$1.39\times10^{-8}$ s^{-1}, blue pathway in Figure 3). We emphasize that the decarbonylation pathways are competitive and that it is difficult to determine the most dominant pathway with DFT. However, clearly, the most dominant decarboxylation pathway, $CH_3CH_2COOCH_3 \rightarrow CH_3CH_2COOCH_2 \rightarrow CH_3CH_2COO+CH_2 \rightarrow \ldots \rightarrow CH_3CH_3+CO_2+CH_4$ (TOF=3.49×10^{-10}) has a TOF that is about 3 orders of magnitude smaller than the competing decarbonylation pathways. Overall, we conclude that the dominant catalytic cycles are decarbonylation pathways and in all of these pathways, dehydrogenation of the α- and β-carbon play an important role in further activating the adsorbed intermediates.

According to the calculated TOFs (Table 2) the main products of the HDO of methyl propionate are predicted to be ethane, ethylene, methanol, and CO. This computational prediction agrees well with a previous experimental study on the HDO of ethyl stearate on Pd/C catalysts by Snåre *et al.*[47] who reported ethanol, n-heptadecane ($C_{17}H_{36}$), and CO to be the main products, while small amounts of C_{17} olefins were also observed.

4.2 Apparent activation barrier, reaction orders, and sensitivity analysis

The apparent activation barrier was computed in the temperature range of 423 to 523 K.

$$E_a = RT^2\left(\frac{\partial \ln(r)}{\partial T}\right)_{p_i} \quad (9)$$

Our model predicts an apparent activation energy of 1.01 eV. This value is slightly higher than the activation barrier of the rate-controlling steps which are in the range of 0.8 to 0.9 eV. A slightly larger apparent activation energy than an activation barrier of an elementary rate-controlling step can be explained with a crowded surface that becomes less crowded at higher temperatures, leading to a further increase in reaction rate.

The reaction order with respect to hydrogen was calculated at 473 K in the range of 0.05 to 0.4 bar. Similarly, the reaction order of methyl propionate and CO were calculated at 473 K and a pressure range of 0.005 to 0.1 bar and 0.0001 to 0.1 bar, respectively.

$$\alpha_i = \left(\frac{\partial \ln(r)}{\partial \ln(p_i)}\right)_{T,p_{j\neq i}} \quad (10)$$

Our model predicts a reaction order with respect to methyl propionate of +1.0, which can be explained by the small methyl propionate coverage in our model. The reaction order with respect to CO is -0.49. This implies that CO is poisoning the surface and an efficient water-gas shift activity of the catalyst is required to remove the CO from the surface and to achieve high

conversion. Finally, the reaction order of H_2 is -0.07, which indicates that under the investigated reaction conditions the hydrogen coverage is balanced with the free site coverage such that the dehydrogenation rates prior to decarbonylation are balanced with the hydrogenation processes required for desorption of the reaction products.

To understand the sensitivity of our model and to determine rate controlling steps and intermediates in the mechanism, we computed Campbell's degrees of rate and thermodynamic control,[48-51] X_{RC} and X_{TRC}.

$$X_{\mathrm{RC},i} = \frac{k_i}{r}\left(\frac{\partial r}{\partial k_i}\right)_{K_i, k_j \neq k_i} \quad , \quad X_{\mathrm{TRC},n} = \frac{1}{r}\left(\frac{\partial r}{\partial\left(\frac{-G_n^0}{RT}\right)}\right)_{G^0_{m\neq n}, G_i^{0,\mathrm{TS}}} \tag{11}$$

where r is the overall rate of reaction, k_i is the forward rate constant for step i, K_i equilibrium constant for step i, R is the gas constant, T denotes the reaction temperature, and G_n^0 is the free energy of adsorbate n. We note that that the degree of rate control for a single rate-determining step in a reaction mechanism is one; and, for transition and intermediate states that do not influence the overall activity, the degrees of thermodynamic and rate control are zero.

The results of our Campbell's degree of rate control analysis suggest that the most controlling steps are propanoyl-methoxy type C-O bond dissociation and dehydrogenation of α-, β-, and methoxy-end carbons of methyl propionate. Reaction 2 ($CH_3CH_2COOCH_3$** + 2*↔ CH_3CH_2CO*** + CH_3O*), propanoyl-methoxy dissociation, is the most rate-controlling C-O bond dissociation step with the X_{RC} of 0.17. Additionally, Reaction 12 ($CH_2CHCOOCH_3$*** + 1* ↔ CH_2CHCO*** +CH_3O*) and Reaction 28 ($CH_3CH_2COOCH_2$*** + 3* ↔ CH_3CH_2CO*** + OCH_2***) are also rate-controlling with the X_{RC} of 0.09 and 0.02 respectively, such that the sum of C-O rate-control is 0.28.

Under the investigated reaction conditions of 473 K and excess of hydrogen, we found that dehydrogenation steps are even more rate-controlling than C-O bond dissociations. Dehydrogenation of the α-carbon of methyl propionate (Reaction 2) is the most rate-controlling dehydrogenation step with an X_{RC} of 0.35. Dehydrogenation of the methoxy-end carbon of methyl propionate (Reaction 5) has an X_{RC} of 0.19, and finally, dehydrogenation of the β-carbon of methyl propionate (Reaction 4) and also dehydrogenation of the β-carbon of $CH_3CHCOOCH_3$*** (Reaction 8: $CH_3CHCOOCH_3$*** + 1* ↔ $CH_2CHCOOCH_3$*** + H*) have a X_{RC} of 0.05 and 0.03 respectively. We note that the sum of the degrees of rate control is slightly smaller than one (0.9) due to numerical inaccuracies of our nonlinear equation solver; however, the trends should not be affected by these numerical issues.

The analysis above suggests the following: Considering that all of the rate-controlling dehydrogenation steps are chemically similar and involve bonding of a hydrogen and carbon atom to the metal surface, we expect that all of these dissociations can be described by one independent activity descriptor, e.g., the dehydrogenation of the α-carbon of methyl propionate. Similarly, all of the rate-controlling C-O bond dissociations are chemically similar and involve bonding of both an oxygen and carbon atom to the metal surface, such that we expect all of these dissociations can be described by another independent activity descriptor, e.g., the C-O dissociation of the propanoyl-methoxy bond.

Finally, the thermodynamic rate control analysis suggests that the adsorption free energy of CO* has a significant effect on the overall rate with X_{TRC} = -0.57 such that destabilizing the adsorbed CO improves the overall reaction rate.

5. Conclusions

The hydrodeoxygenation of methyl propionate was investigated over a Pd (111) surface model from first principles. An extensive network of elementary reactions was studied and a microkinetic model was developed to study the reaction mechanism at a reaction temperature of 473K. We found the most dominant pathway to involve methyl propionate to undergo two dehydrogenation steps of both its α and β-carbon to form $CH_2CHCOOCH_3$ followed by a C-O bond dissociation to form CH_2CHCO and OCH_3, next, CH_2CHCO goes through C-C bond cleavage to produce C2 hydrocarbons. Surface methoxy species get hydrogenated to form methanol, i.e., the most dominant pathway is $CH_3CH_2COOCH_3 \rightarrow CH_3CHCOOCH_3 \rightarrow CH_2CHCOOCH_3 \rightarrow CH_2CHCO+OCH_3 \rightarrow \ldots \rightarrow CH_3CH_3+CO+CH_3OH$, TOF=$1.85\times10^{-7}$ s^{-1}. Decarbonylation is the dominant mechanism and methanol, CO, and C_2 hydrocarbons are predicted to be the main reaction products of the HDO of methyl propionate over Pd (111). H, CO, and CH_3C were identified to be the most abundant surface intermediates. The apparent activation barrier was calculated to be 1.01 eV. Finally, our sensitivity analysis suggests that dehydrogenation of α-carbon of methyl propionate and the propanoyl-methoxy bond dissociation are rate-controlling steps and possible activity descriptors.

6. Acknowledgements

This work has been supported by the National Science Foundation under Grant No. CBET-1159863 and in part by the USC future fuels program and USC NanoCenter. Computational resources have been provided by the National Energy Research Scientific Computing Center (NERSC) which is supported by the Office of Science of the U.S. Department of Energy and in part by XSEDE resources provided by the National Institute for Computational Sciences (NICS), Texas advanced Computing Center (TACC), and the Purdue University under grant number TG-

CTS090100. Finally, computing resources from the USC NanoCenter and USC's High Performance Computing Group are gratefully acknowledged.

TABLE 1. Zero-point energy corrected activation barriers, reaction energies, transition-state imaginary frequencies, and TS bond lengths of all elementary steps investigated for the HDO of methyl propionate. * symbolizes an active site and ** symbolizes two occupied active sites, etc.

#	Reaction	E_{act} (eV)	ΔE_0 (eV)	ν (cm^{-1})	TS bond (Å)
Step 1	$CH_3CH_2COOCH_3$** + 1* ↔ CH_3CH_2COO** + CH_3*	1.54	-0.45	521 *i*	2.08
Step 2	$CH_3CH_2COOCH_3$** + 2*↔ CH_3CH_2CO*** + CH_3O*	0.73	0.19	161 *i*	2.05
Step 3	$CH_3CH_2COOCH_3$** + 2* ↔ $CH_3CHCOOCH_3$*** + H*	0.70	-0.07	950 *i*	1.55
Step 4	$CH_3CH_2COOCH_3$** + 2* ↔ $CH_2CH_2COOCH_3$*** + H*	0.78	0.12	776 *i*	1.59
Step 5	$CH_3CH_2COOCH_3$** + 2* ↔ $CH_3CH_2COOCH_2$*** + H*	0.72	0.02	844 *i*	1.56
Step 6	$CH_3CHCOOCH_3$*** + 1* ↔ CH_3CHCOO*** + CH_3*	1.63	0.00	539 *i*	2.02
Step 7	$CH_3CHCOOCH_3$*** + 1* ↔ CH_3CHCO*** + CH_3O*	0.74	0.27	187 *i*	2.08
Step 8	$CH_3CHCOOCH_3$*** + 1* ↔ $CH_2CHCOOCH_3$*** + H*	0.46	-0.47	1019 *i*	1.51
Step 9	$CH_3CHCOOCH_3$*** + 1* ↔ $CH_3CHCOOCH_2$*** + H*	0.75	-0.02	856 *i*	1.53
Step 10	$CH_2CHCOOCH_3$*** + 2* ↔ $CH_2CHCOOCH_2$**** + H*	0.96	0.13	958 *i*	1.54
Step 11	$CH_2CHCOOCH_3$*** + 2* ↔ $CHCHCOOCH_3$**** + H*	0.85	0.03	743 *i*	1.79
Step 12	$CH_2CHCOOCH_3$*** + 1* ↔ CH_2CHCO*** +CH_3O*	0.91	0.41	241 *i*	2.09
Step 13	$CH_3CHCOOCH_2$*** + 2* ↔ $CH_2CHCOOCH_2$**** + H*	0.38	-0.33	951 *i*	1.54
Step 14	$CH_3CHCOOCH_2$*** + 3* ↔ CH_3CHCO*** + OCH_2***	0.47	-0.19	252 *i*	1.97
Step 15	$CHCHCOOCH_3$**** + 2* ↔ CHCH*** + $COOCH_3$***	0.91	-0.06	453 *i*	2.00
Step 16	$CH_2CHCOOCH_2$**** + 3* → CH_2CH*** + $COOCH_2$****	0.93	0.01	335 *i*	2.09
Step 17	$CH_2CHCOOCH_2$**** + 2* ↔ CH_2CHCO*** + OCH_2***	0.47	-0.20	222 *i*	2.06
Step 18	$CH_2CH_2COOCH_3$*** + 1* ↔ $CH_2CHCOOCH_3$*** + H*	0.34	-0.67	965 *i*	1.49
Step 19	$CH_2CH_2COOCH_3$*** + 1* ↔ $CH_2CH_2COOCH_2$*** + H*	0.83	0.00	1037 *i*	1.54
Step 20	$CH_2CH_2COOCH_3$*** + 2* ↔ CH_2CH_2** + $COOCH_3$***	0.98	-0.42	429 *i*	2.04
Step 21	$CH_2CH_2COOCH_3$*** + 1* ↔ CH_2CH_2CO*** + CH_3O*	0.58	0.20	190 *i*	2.05
Step 22	$CH_2CH_2COOCH_2$*** + 1* ↔ $CH_2CHCOOCH_2$**** + H*	0.67	-0.54	993 *i*	1.61

Step 23	$CH_2CH_2COOCH_2$*** + 3* ↔ CH_2CH_2** +$COOCH_2$****	0.91	-0.55	453 *i*	2.05
Step 24	$CH_2CH_2COOCH_2$*** + 3* ↔ CH_2CH_2CO*** + OCH_2***	0.26	-0.30	244 *i*	1.88
Step 25	$CH_3CH_2COOCH_2$*** + 1* ↔ $CH_3CHCOOCH_2$*** + H*	0.59	-0.11	750 *i*	1.59
Step 26	$CH_3CH_2COOCH_2$*** + 1* ↔ $CH_2CH_2COOCH_2$*** + H*	0.89	0.10	670 *i*	1.64
Step 27	$CH_3CH_2COOCH_2$*** + 1* ↔ CH_3CH_2COO** + CH_2**	0.70	-0.57	217 *i*	2.30
Step 28	$CH_3CH_2COOCH_2$*** + 3* ↔ CH_3CH_2CO*** + OCH_2***	0.15	-0.31	259 *i*	1.82
Step 29	CH_3CH_2CO*** + 1* ↔ CH_3CHCO*** + H*	0.81	0.01	901 *i*	1.57
Step 30	CH_3CH_2CO*** ↔ CH_3CH_2* + CO* + 1*	1.01	-0.60	372 *i*	2.34
Step 31	CH_3CHCO*** + 1* ↔ CH_2CHCO*** + H*	0.46	-0.34	766 *i*	1.47
Step 32	CH_3CHCO*** ↔ CH_3CH** + CO*	1.02	-0.81	410 *i*	2.30
Step 33	CH_3CHCO*** + 1* ↔ CH_3CCO*** + H*	0.52	-0.38	848 *i*	1.66
Step 34	CH_2CHCO*** + 1* ↔ CH_2CH*** + CO*	0.78	-0.74	491 *i*	1.98
Step 35	CH_2CHCO*** + 2* ↔ $CHCHCO$**** + H*	0.68	0.01	631 *i*	1.59
Step 36	$CHCHCO$**** ↔ CHCH*** + CO*	0.57	-1.09	462 *i*	2.05
Step 37	CH_3CCO*** ↔ CH_3C* + CO* + 1*	0.44	-1.37	396 *i*	1.73
Step 38	CH_2CH_2CO*** ↔ CH_2CH_2** + CO*	0.76	-1.22	471 *i*	2.13
Step 39	CH_2CH_2CO*** + 1* ↔ CH_2CHCO *** + H*	0.66	-0.46	942 *i*	1.61
Step 40	$COOCH_3$*** + 2* ↔ $COOCH_2$*** + H*	0.58	-0.13	900 *i*	1.56
Step 41	$COOCH_3$*** ↔ CO* + CH_3O* + 1*	0.56	-0.60	205 *i*	2.04
Step 42	$COOCH_3$*** ↔ CO_2* + CH_3* + 1*	1.48	-0.38	554 *i*	1.92
Step 43	$COOCH_2$**** ↔ CO* + OCH_2***	0.29	-0.95	345 *i*	1.78
Step 44	$COOCH_2$**** ↔ CO_2* + CH_2** + 1*	0.89	-0.35	432 *i*	2.03
Step 45	CHCH*** + H* ↔ CH_2CH*** + 1*	0.82	0.30	1025 *i*	1.57
Step 46	CH_2CH*** ↔ CH_2C** + H*	0.46	-0.43	970 *i*	1.48
Step 47	CH_2C**+H* ↔ CH_3C** + 2*	0.88	-0.23	966 *i*	1.70
Step 48	CH_2CH*** + H* ↔ CH_2CH_2** + 2*	0.88	-0.02	787 *i*	1.75
Step 49	CH_2CH*** + H* ↔ CH_3CH** + 2*	0.79	0.26	982 *i*	1.55

Step 50	$CH_3C^{***} + H^* \leftrightarrow CH_3CH^{**} + 2^*$	1.11	0.94	196 *i*	1.13
Step 51	$CH_3CH^{**} + H^* \leftrightarrow CH_3CH_2^* + 2^*$	0.86	0.21	801 *i*	1.69
Step 52	$CH_2CH_2^{**} + H^* \leftrightarrow CH_3CH_2^* + 2^*$	0.88	0.48	924 *i*	1.53
Step 53	$CH_3CH_2^* + H^* \leftrightarrow CH_3CH_3^* + 1^*$	0.60	0.04	941 *i*	1.59
Step 54	$CH_3O^* + 3^* \leftrightarrow CH_2O^{***} + H^*$	0.44	-0.48	914 *i*	1.46
Step 55	$CH_2O^{***} + 1^* \leftrightarrow CHO^{***} + H^*$	0.67	-0.87	603 *i*	1.64
Step 56	$CHO^{***} \leftrightarrow CO^* + H^* + 1^*$	0.16	-1.42	684 *i*	1.36
Step 57	$CH_3O^* + H^* \leftrightarrow CH_3OH^* + 1^*$	0.60	0.01	726 *i*	1.61
Step 58	$CH_2^{**} + H^* \leftrightarrow CH_3^* + 2^*$	0.78	0.10	788 *i*	1.84
Step 59	$CH_3^* + H^* \leftrightarrow CH_4^* + 1^*$	0.58	-0.03	938 *i*	1.57
Step 60	$CH_3CH_2COO^{**} \leftrightarrow CH_3CH_2^* + CO_2^*$	1.43	0.24	435 *i*	1.93
Step 61	$CH_3CH_2COO^{**} + 2^* \leftrightarrow CH_3CHCOO^{***} + H^*$	1.22	0.38	811 *i*	1.64
Step 62	$CH_3CHCOO^{***} + \leftrightarrow CH_3CH^{**} + CO_2^*$	0.96	-0.32	449 *i*	2.10
Step 63	$CH_3CHCOO^{***} + 1^* \leftrightarrow CH_3CCOO^{***} + H^*$	0.85	-0.08	784 *i*	1.75
Step 64	$CH_3CCOO^{***} \leftrightarrow CH_3C^* + CO_2^* + 1^*$	0.65	-1.17	575 *i*	2.09
Step 65	$CH_3CH_2COOCH_3 + 2^* \leftrightarrow CH_3CH_2COOCH_3^{**}$	N/A	-0.52	N/A	N/A
Step 66	$CH_3CH_3 + 1^* \leftrightarrow CH_3CH_3^*$	N/A	-0.17	N/A	N/A
Step 67	$CH_2CH_2 + 2^* \leftrightarrow CH_2CH_2^{**}$	N/A	-0.98	N/A	N/A
Step 68	$CHCH + 3^* \leftrightarrow CHCH^{***}$	N/A	-1.67	N/A	N/A
Step 69	$CH_4 + 1^* \leftrightarrow CH_4^*$	N/A	-0.08	N/A	N/A
Step 70	$CH_3OH + 1^* \leftrightarrow CH_3OH^*$	N/A	-0.32	N/A	N/A
Step 71	$CO + 1^* \leftrightarrow CO^*$	N/A	-1.97	N/A	N/A
Step 72	$CO_2 + 1^* \leftrightarrow CO_2^*$	N/A	0.02	N/A	N/A
Step 73	$H_2 + 2^* \rightarrow 2H^*$	N/A	-1.13	N/A	N/A

TABLE 2. Equilibrium, forward rate constants, and calculated net rate (turnover frequency) for the elementary steps in the HDO of methyl propionate over Pd (111) model surfaces at a temperature of 473 K.

	Reaction	K_{eq}	k_f (s^{-1})	TOF (s^{-1})
Step 1	$CH_3CH_2COOCH_3$** + 1* ↔ CH_3CH_2COO** + CH_3*	1.08×10^{-5}	2.08×10^{-4}	6.17×10^{-15}
Step 2	$CH_3CH_2COOCH_3$** + 2*↔ CH_3CH_2CO*** + CH_3O*	7.63×10^{-3}	3.96×10^{4}	6.43×10^{-8}
Step 3	$CH_3CH_2COOCH_3$** + 2* ↔ $CH_3CHCOOCH_3$*** + H*	1.52	1.37×10^{5}	1.85×10^{-7}
Step 4	$CH_3CH_2COOCH_3$** + 2* ↔ $CH_2CH_2COOCH_3$*** + H*	1.91×10^{-2}	1.01×10^{4}	1.39×10^{-8}
Step 5	$CH_3CH_2COOCH_3$** + 2* ↔ $CH_3CH_2COOCH_2$*** + H*	9.81×10^{-2}	5.02×10^{4}	7.85×10^{-8}
Step 6	$CH_3CHCOOCH_3$*** + 1* ↔ CH_3CHCOO*** + CH_3*	2.41	4.00×10^{-5}	1.35×10^{-18}
Step 7	$CH_3CHCOOCH_3$*** + 1* ↔ CH_3CHCO*** + CH_3O*	2.49×10^{-3}	1.30×10^{5}	4.37×10^{-9}
Step 8	$CH_3CHCOOCH_3$*** + 1* ↔ $CH_2CHCOOCH_3$*** + H*	3.98×10^{4}	4.64×10^{7}	1.80×10^{-7}
Step 9	$CH_3CHCOOCH_3$*** + 1* ↔ $CH_3CHCOOCH_2$*** + H*	4.89×10^{-1}	3.04×10^{4}	9.07×10^{-10}
Step 10	$CH_2CHCOOCH_3$*** + 2* ↔ $CH_2CHCOOCH_2$**** + H*	1.27×10^{-2}	2.69×10^{2}	1.39×10^{-9}
Step 11	$CH_2CHCOOCH_3$*** + 2* ↔ $CHCHCOOCH_3$**** + H*	1.90×10^{-1}	5.29×10^{3}	1.25×10^{-11}
Step 12	$CH_2CHCOOCH_3$*** + 1* ↔ CH_2CHCO*** +CH_3O*	1.28×10^{-4}	1.98×10^{3}	1.92×10^{-7}
Step 13	$CH_3CHCOOCH_2$*** + 2* ↔ $CH_2CHCOOCH_2$**** + H*	1.03×10^{3}	2.69×10^{8}	1.76×10^{-9}
Step 14	$CH_3CHCOOCH_2$*** + 3* ↔ CH_3CHCO*** + OCH_2***	3.77×10^{2}	1.10×10^{8}	5.01×10^{-11}
Step 15	$CHCHCOOCH_3$**** + 2* ↔ CHCH*** + $COOCH_3$***	1.24×10^{1}	2.77×10^{3}	1.25×10^{-11}
Step 16	$CH_2CHCOOCH_2$**** + 3* ↔ CH_2CH*** + $COOCH_2$****	2.59	6.95×10^{2}	3.12×10^{-16}
Step 17	$CH_2CHCOOCH_2$**** + 2* ↔ CH_2CHCO*** + OCH_2***	7.51×10^{2}	3.84×10^{8}	3.15×10^{-9}
Step 18	$CH_2CH_2COOCH_3$*** + 1* ↔ $CH_2CHCOOCH_3$*** + H*	3.17×10^{6}	8.55×10^{8}	1.30×10^{-8}
Step 19	$CH_2CH_2COOCH_3$*** + 1* ↔ $CH_2CH_2COOCH_2$*** + H*	1.14×10^{-1}	1.93×10^{3}	7.42×10^{-13}
Step 20	$CH_2CH_2COOCH_3$*** + 2* ↔ CH_2CH_2** + $COOCH_3$***	3.87×10^{4}	9.87×10^{1}	2.09×10^{-15}

Step 21	$CH_2CH_2COOCH_3$*** + 1* ↔ CH_2CH_2CO*** + CH_3O*	7.44×10^{-3}	2.41×10^{6}	9.34×10^{-10}
Step 22	$CH_2CH_2COOCH_2$*** + 1* ↔ $CH_2CHCOOCH_2$**** + H*	3.52×10^{5}	8.95×10^{5}	-3.23×10^{-15}
Step 23	$CH_2CH_2COOCH_2$*** + 3* ↔ CH_2CH_2** +$COOCH_2$****	5.74×10^{6}	3.30×10^{3}	2.85×10^{-19}
Step 24	$CH_2CH_2COOCH_2$*** + 3* ↔ CH_2CH_2CO*** + OCH_2***	8.44×10^{3}	1.18×10^{10}	1.02×10^{-12}
Step 25	$CH_3CH_2COOCH_2$*** + 1* ↔ $CH_3CHCOOCH_2$*** + H*	7.56	3.86×10^{6}	9.06×10^{-10}
Step 26	$CH_3CH_2COOCH_2$*** + 1* ↔ $CH_2CH_2COOCH_2$*** + H*	2.22×10^{-2}	5.89×10^{2}	2.73×10^{-13}
Step 27	$CH_3CH_2COOCH_2$*** + 1* ↔ CH_3CH_2COO** + CH_2**	2.74×10^{6}	7.28×10^{5}	3.49×10^{-10}
Step 28	$CH_3CH_2COOCH_2$*** + 3* ↔ CH_3CH_2CO*** + OCH_2***	8.01×10^{3}	5.37×10^{10}	7.72×10^{-8}
Step 29	CH_3CH_2CO*** + 1* ↔ CH_3CHCO*** + H*	3.08×10^{-1}	7.47×10^{3}	1.05×10^{-7}
Step 30	CH_3CH_2CO*** ↔ CH_3CH_2* + CO* + 1*	4.73×10^{6}	1.36×10^{2}	3.61×10^{-8}
Step 31	CH_3CHCO*** + 1* ↔ CH_2CHCO*** + H*	2.06×10^{3}	5.51×10^{7}	-6.17×10^{-8}
Step 32	CH_3CHCO*** ↔ CH_3CH** + CO*	6.68×10^{8}	3.55×10^{2}	6.62×10^{-11}
Step 33	CH_3CHCO*** + 1* ↔ CH_3CCO*** + H*	1.05×10^{4}	1.68×10^{7}	1.71×10^{-7}
Step 34	CH_2CHCO*** + 1* ↔ CH_2CH*** + CO*	6.37×10^{7}	3.06×10^{4}	5.85×10^{-8}
Step 35	CH_2CHCO*** + 2* ↔ $CHCHCO$**** + H*	9.03×10^{-1}	5.54×10^{5}	5.83×10^{-8}
Step 36	$CHCHCO$**** ↔ $CHCH$*** + CO*	7.59×10^{11}	5.57×10^{6}	5.83×10^{-8}
Step 37	CH_3CCO*** ↔ CH_3C* + CO* + 1*	1.00×10^{15}	1.76×10^{8}	1.71×10^{-7}
Step 38	CH_2CH_2CO*** ↔ CH_2CH_2** + CO*	2.19×10^{13}	1.81×10^{5}	9.85×10^{-10}
Step 39	CH_2CH_2CO*** + 1* ↔ CH_2CHCO *** + H*	5.46×10^{4}	3.89×10^{5}	-4.99×10^{-11}
Step 40	$COOCH_3$*** + 2* ↔ $COOCH_2$*** + H*	1.69×10^{1}	1.42×10^{6}	3.02×10^{-15}
Step 41	$COOCH_3$*** ↔ CO* + CH_3O* + 1*	4.20×10^{6}	1.77×10^{7}	1.25×10^{-11}
Step 42	$COOCH_3$*** ↔ CO_2* + CH_3* + 1*	1.21×10^{5}	1.87×10^{-3}	1.33×10^{-21}
Step 43	$COOCH_2$**** ↔ CO* + OCH_2***	1.85×10^{10}	1.75×10^{10}	3.36×10^{-15}
Step 44	$COOCH_2$**** ↔ CO_2* + CH_2** + 1*	1.11×10^{4}	3.62×10^{3}	7.89×10^{-21}
Step 45	$CHCH$*** + H* ↔ CH_2CH*** + 1*	8.26×10^{-4}	2.03×10^{4}	5.83×10^{-8}

Step 46	$CH_2CH^{***} \leftrightarrow CH_2C^{**} + H^*$	3.07×10^{4}	1.73×10^{8}	-2.39×10^{-7}
Step 47	$CH_2C^{**}+H^* \leftrightarrow CH_3C^{**} + 2^*$	8.27×10^{2}	5.44×10^{3}	-2.39×10^{-7}
Step 48	$CH_2CH^{***} + H^* \leftrightarrow CH_2CH_2^{**} + 2^*$	6.28	5.64×10^{3}	2.08×10^{-7}
Step 49	$CH_2CH^{***} + H^* \leftrightarrow CH_3CH^{**} + 2^*$	5.10×10^{-3}	3.71×10^{4}	1.48×10^{-7}
Step 50	$CH_3C^{***} + H^* \leftrightarrow CH_3CH^{**} + 2^*$	6.32×10^{-11}	3.50	-1.12×10^{-7}
Step 51	$CH_3CH^{**} + H^* \leftrightarrow CH_3CH_2^* + 2^*$	2.30×10^{-2}	1.74×10^{4}	3.60×10^{-8}
Step 52	$CH_2CH_2^{**} + H^* \leftrightarrow CH_3CH_2^* + 2^*$	2.05×10^{-5}	3.54×10^{3}	-2.31×10^{-8}
Step 53	$CH_3CH_2^* + H^* \leftrightarrow CH_3CH_3^* + 1^*$	2.18	3.67×10^{6}	1.10×10^{-7}
Step 54	$CH_3O^* + 3^* \leftrightarrow CH_2O^{***} + H^*$	7.42×10^{4}	1.02×10^{8}	1.45×10^{-8}
Step 55	$CH_2O^{***} + 1^* \leftrightarrow CHO^{***} + H^*$	1.20×10^{9}	9.66×10^{6}	9.49×10^{-8}
Step 56	$CHO^{***} \leftrightarrow CO^* + H^* + 1^*$	9.35×10^{14}	1.24×10^{12}	9.49×10^{-8}
Step 57	$CH_3O^* + H^* \leftrightarrow CH_3OH^* + 1^*$	5.74×10^{-2}	4.23×10^{5}	2.47×10^{-7}
Step 58	$CH_2^{**} + H^* \leftrightarrow CH_3^* + 2^*$	6.45×10^{-1}	1.12×10^{5}	3.49×10^{-10}
Step 59	$CH_3^* + H^* \leftrightarrow CH_4^* + 1^*$	4.38×10^{1}	1.50×10^{7}	3.49×10^{-10}
Step 60	$CH_3CH_2COO^{**} \leftrightarrow CH_3CH_2^* + CO_2^*$	1.75×10^{-2}	2.49×10^{-2}	6.09×10^{-8}
Step 61	$CH_3CH_2COO^{**} + 2^* \leftrightarrow CH_3CHCOO^{***} + H^*$	2.14×10^{-5}	2.46×10^{-1}	3.49×10^{-10}
Step 62	$CH_3CHCOO^{***} + \leftrightarrow CH_3CH^{**} + CO_2^*$	1.50×10^{4}	1.41×10^{3}	2.67×10^{-10}
Step 63	$CH_3CHCOO^{***} + 1^* \leftrightarrow CH_3CCOO^{***} + H^*$	8.51	7.97×10^{3}	8.25×10^{-11}
Step 64	$CH_3CCOO^{***} \leftrightarrow CH_3C^* + CO_2^* + 1^*$	1.04×10^{13}	1.65×10^{6}	8.25×10^{-11}
Step 65	$CH_3CH_2COOCH_3 + 2^* \leftrightarrow CH_3CH_2COOCH_3^{**}$	1.81×10^{-5}	8.73×10^{7}	3.42×10^{-7}
Step 66	$CH_3CH_3 + 1^* \leftrightarrow CH_3CH_3^*$	2.79×10^{-7}	1.50×10^{8}	1.10×10^{-7}
Step 67	$CH_2CH_2 + 2^* \leftrightarrow CH_2CH_2^{**}$	2.79×10^{1}	1.55×10^{8}	2.32×10^{-7}
Step 68	$CHCH + 3^* \leftrightarrow CHCH^{***}$	2.59×10^{12}	1.61×10^{8}	5.29×10^{-14}
Step 69	$CH_4 + 1^* \leftrightarrow CH_4^*$	8.51×10^{-6}	2.05×10^{8}	3.49×10^{-10}
Step 70	$CH_3OH + 1^* \leftrightarrow CH_3OH^*$	5.89×10^{-5}	1.45×10^{8}	2.47×10^{-7}

Step 71	$CO + 1* \leftrightarrow CO*$	5.33×10^{12}	1.55×10^{8}	Equilibrium
Step 72	$CO_2 + 1* \leftrightarrow CO_2*$	2.79×10^{-6}	1.30×10^{8}	3.49×10^{-10}
Step 73	$H_2 + 2* \rightarrow 2H*$	1.65×10^{6}	5.80×10^{8}	Equilibrium

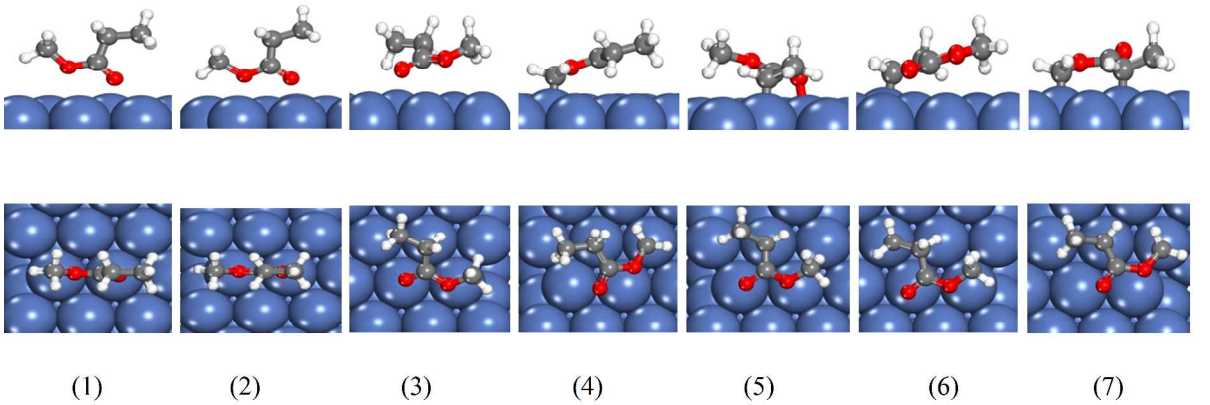

(1) (2) (3) (4) (5) (6) (7)

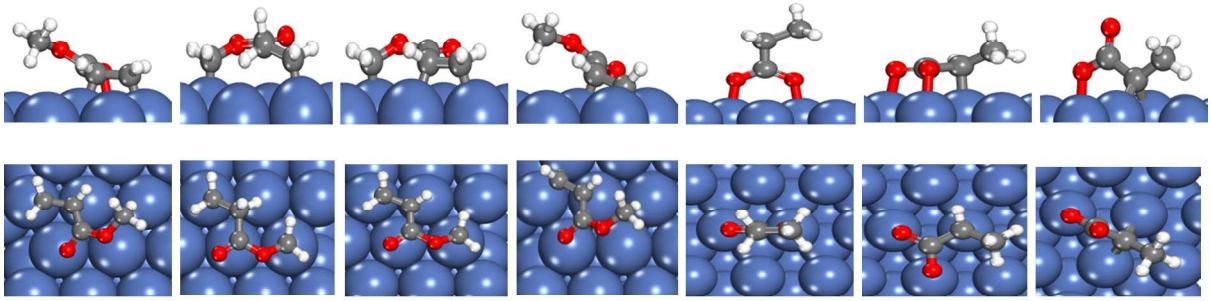

(8) (9) (10) (11) (12) (13) (14)

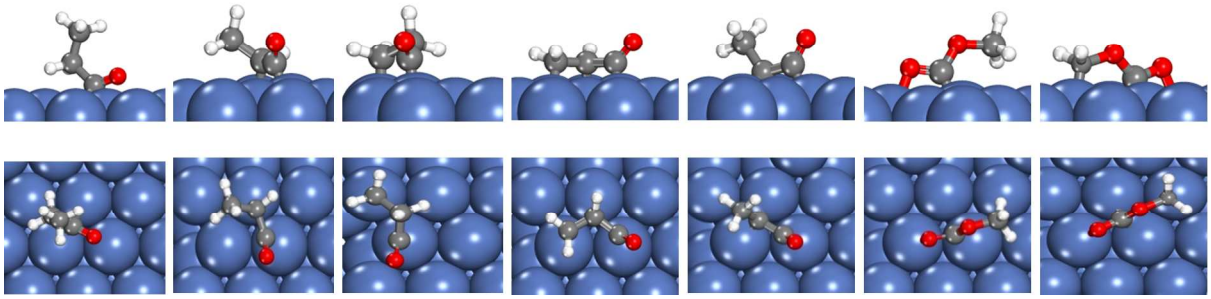

(15) (16) (17) (18) (19) (20) (21)

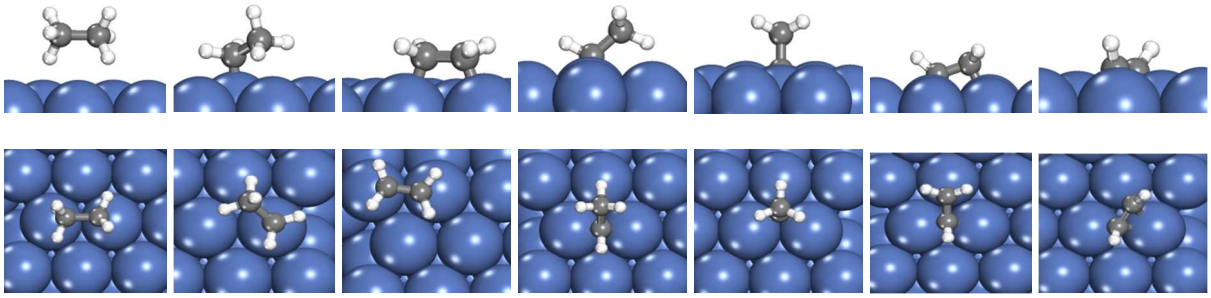

(22) (23) (24) (25) (26) (27) (28)

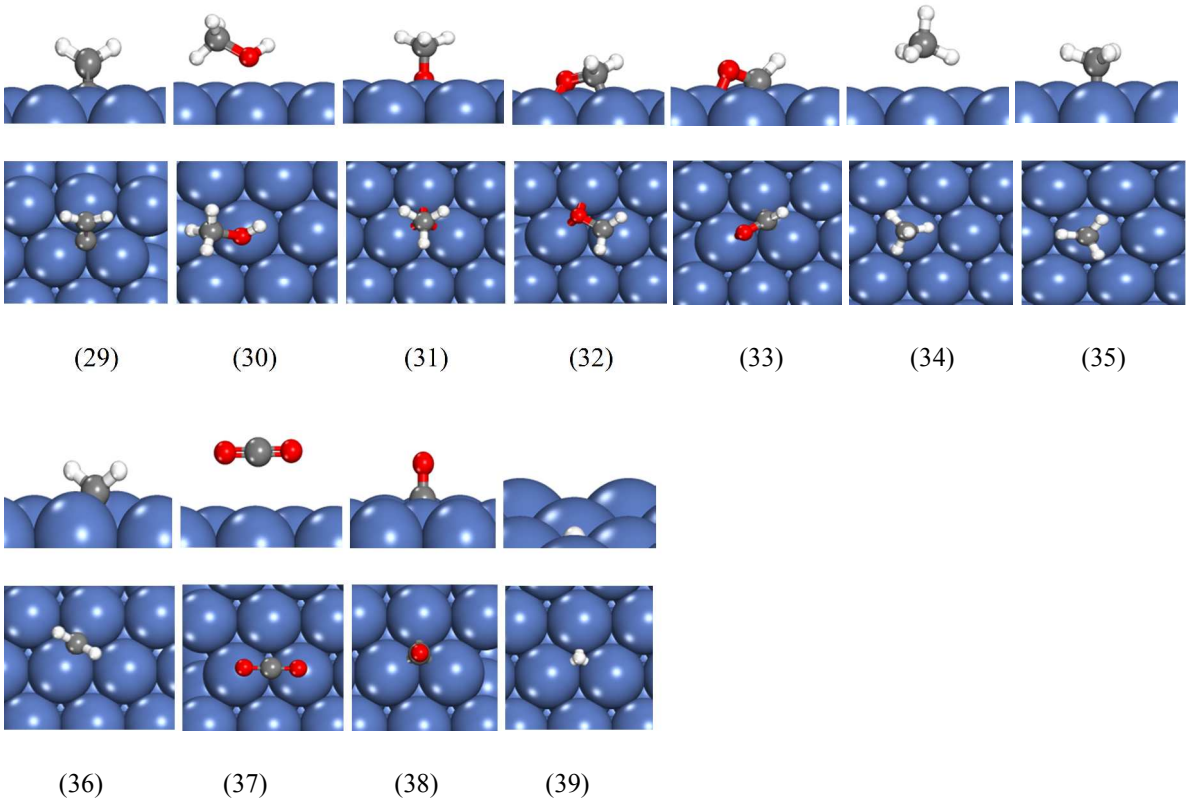

Figure 1. Side and top view of most stable adsorption structure of intermediates involved in HDO of methyl propionate over Pd (111). (1) Methyl Propionate-Cis ($CH_3CH_2COOCH_3$); (2) Methyl Propionate-Trans ($CH_3CH_2COOCH_3$); (3) Methyl Propionate-Chair ($CH_3CH_2COOCH_3$); (4) Methylene Propionate ($CH_3CH_2COOCH_2$); (5) Methylcarboxylethyledene ($CH_3CHCOOCH_3$); (6) Methylcarboxylethene ($CH_2CH_2COOCH_3$); (7) Methylenecarboxylethyledne ($CH_3CHCOOCH_2$); (8) Methylcarboxylvinyl ($CH_2CHCOOCH_3$); (9) Methylenecarboxylethene ($CH_2CH_2COOCH_2$); (10) Methylenecarboxylvinyl ($CH_2CHCOOCH_2$); (11) Methylcarboxylethyne ($CHCHCOOCH_3$); (12)Propionate (CH_3CH_2COO); (13) Carboxylethylidene (CH_3CHCOO); (14) Carboxylethenyl (CH_3CCOO); (15) Propanoyl (CH_3CH_2CO); (16) Carbonylethylidene (CH_3CHCO); (17) Carbonylethene (CH_2CH_2CO); (18) Carbonylvinyl (CH_2CHCO); (19) Carbonylethenyl (CH_3CCO); (20) carboxylmethyl ($COOCH_3$); (21) carboxylmethylene ($COOCH_2$); (22) Ethane (CH_3CH_3); (23) Ethyl (CH_3CH_2); (24) Ethene (CH_2CH_2); (25) Ethylidene (CH_3CH); (26) Ethenyl (CH_3C); (27) Vinyl CH_2CH; (28) Ethyne (CHCH); (29) CH_2C; (30) Methanol (CH_3OH); (31) Methoxy (CH_3O); (32) Formaldehyde (CH_2O); (33) Formyl (CHO); (34) Methane (CH_4); (35) Methyl (CH_3); (36) Methylene (CH_2); (37) Carbon dioxide (CO_2); (38) Carbon monoxide(CO); (39)Hydrogen atom(H);

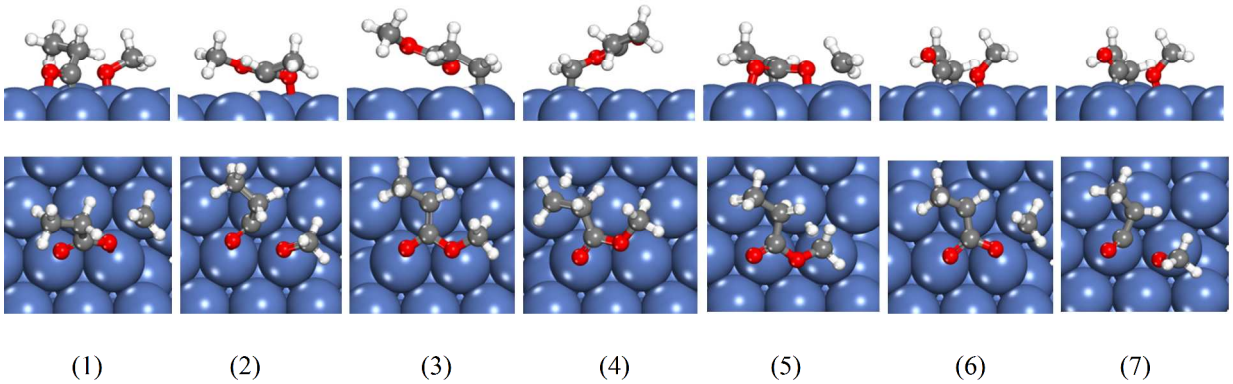

(1) (2) (3) (4) (5) (6) (7)

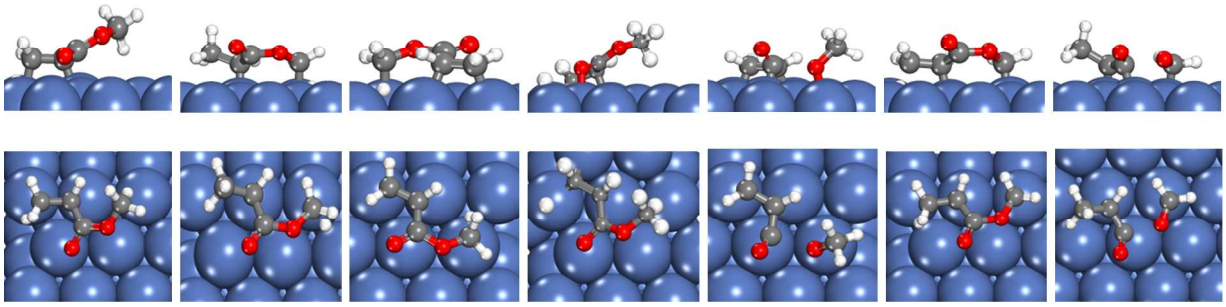

(8) (9) (10) (11) (12) (13) (14)

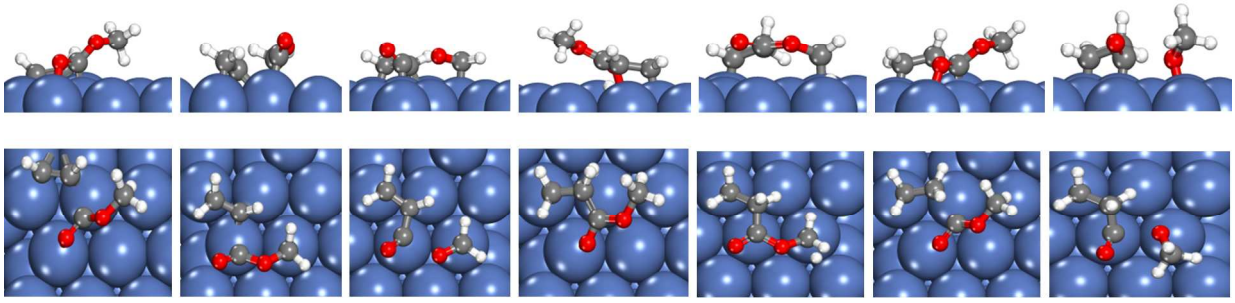

(15) (16) (17) (18) (19) (20) (21)

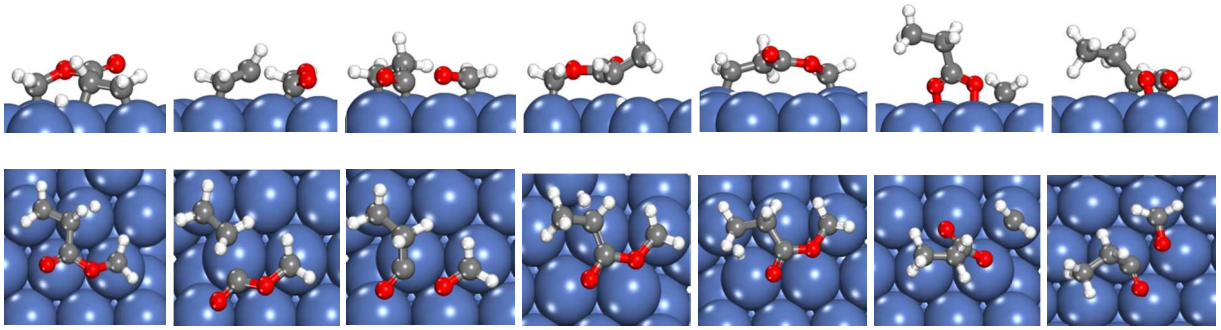

(22) (23) (24) (25) (26) (27) (28)

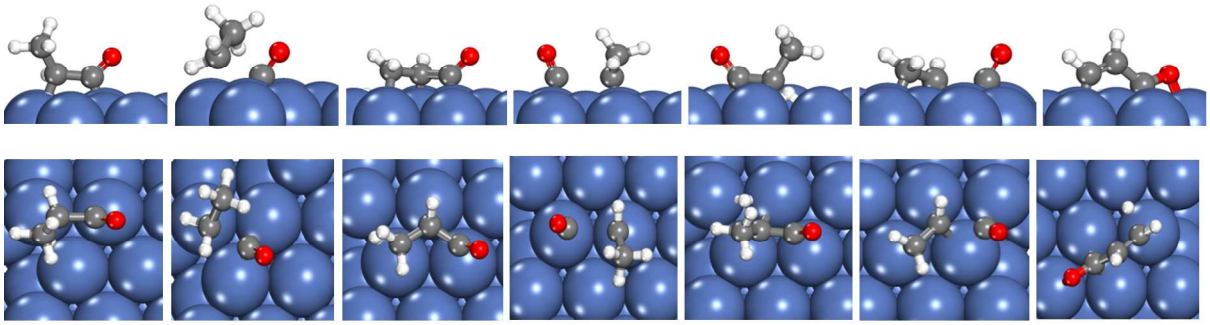

(29) (30) (31) (32) (33) (34) (35)

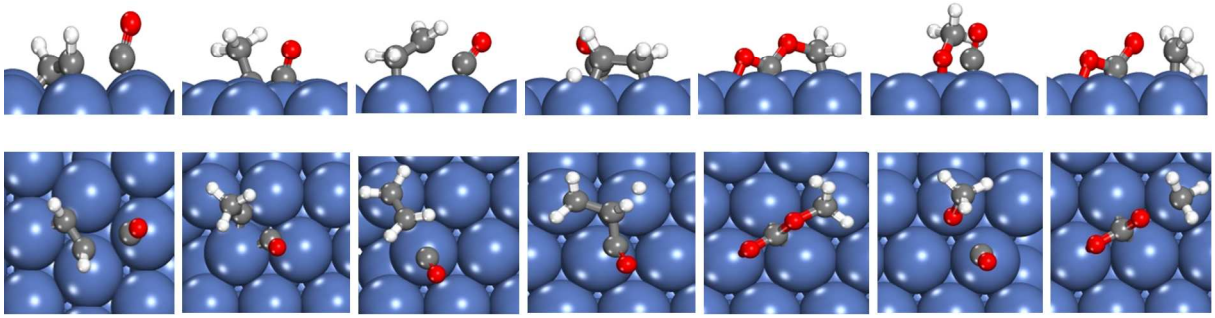

(36) (37) (38) (39) (40) (41) (42)

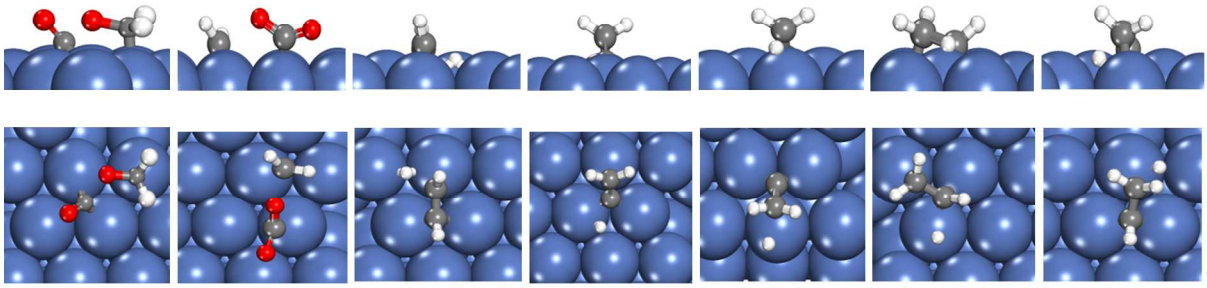

(43) (44) (45) (46) (47) (48) (49)

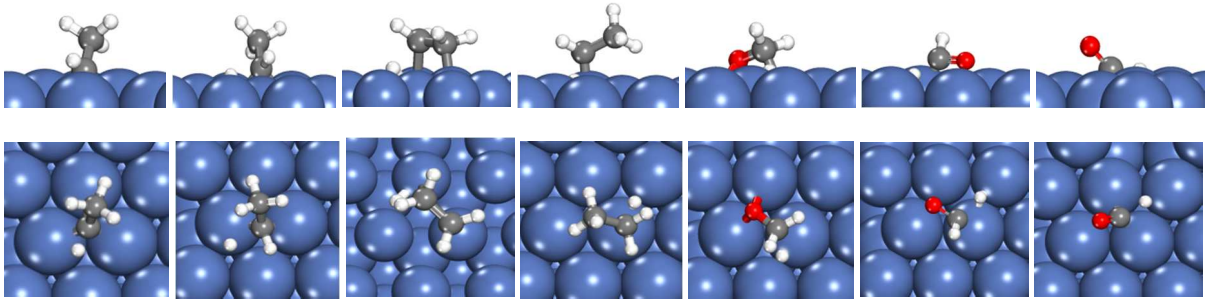

(50) (51) (52) (53) (54) (55) (56)

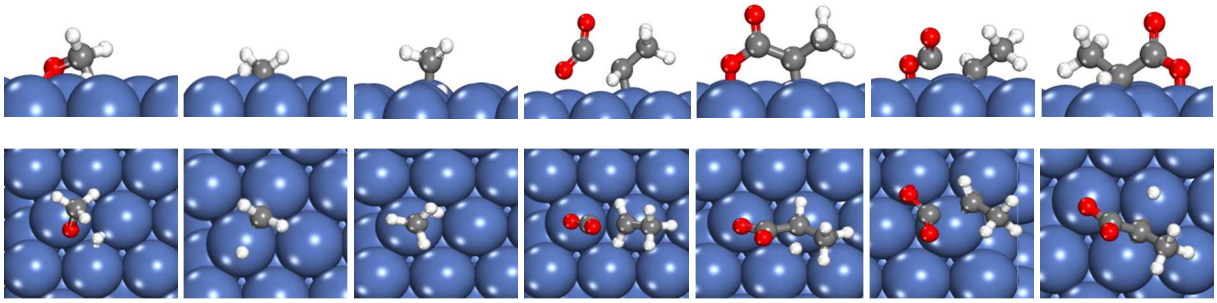

(57) (58) (59) (60) (61) (62) (63)

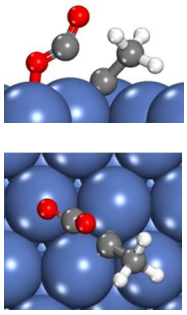

(64)

Figure 2. Snapshots of transition states of the elementary reactions involved in hydrodeoxygenation of methyl propionate on Pd (111) surface. Upper panels are for side views and lower ones for top views. Numbers correspond to the reaction numbers shown in Table 1.

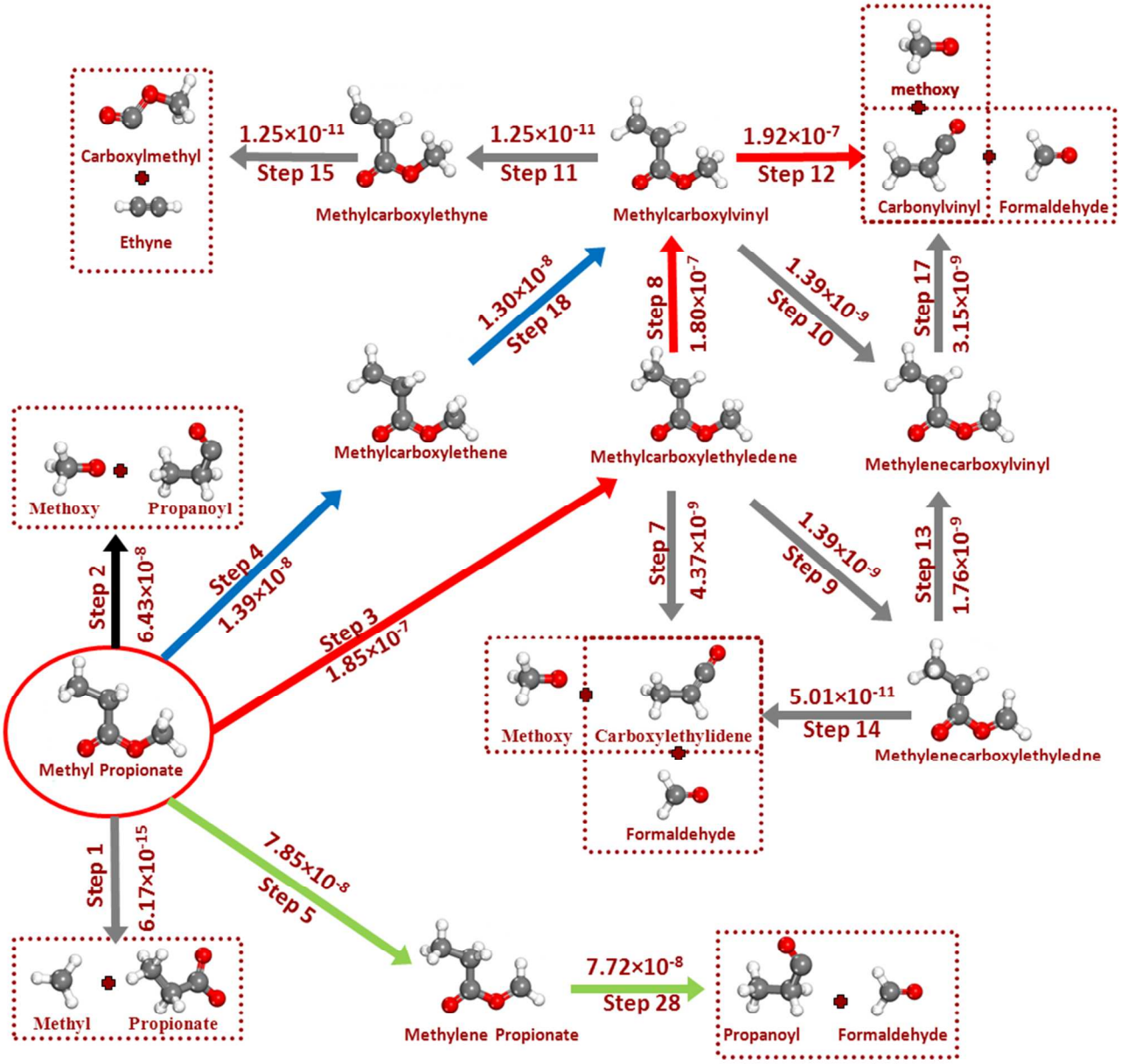

Figure 3. Schematic representation of the most important reaction pathways in the network considered in the HDO of methyl propionate over Pd (111). We note that in our microkinetic calculations, we included all the elementary steps illustrated in Table 1; however, this Figure is a schematic of elementary steps involved in the dominant pathways of the HDO of methyl propionate. TOFs (s^{-1}) shown for various elementary steps are computed at a temperature of 473 K, a methyl propionate gas phase pressure of 0.01 bar and a hydrogen partial pressure of 0.2 bar. TOFs (s^{-1}) for elementary reactions not shown in this figure are illustrated in Table 2. The most dominant pathway is shown in red color ($CH_3CH_2COOCH_3 \rightarrow CH_3CHCOOCH_3 \rightarrow CH_2CHCOOCH_3 \rightarrow CH_2CHCO+OCH_3 \rightarrow \ldots \rightarrow CH_3CH_3+CO+CH_3OH$). Other competitive pathways are shown in black, blue, and green. Reaction pathways of the intermediates shown in rectangles are explained in detail in sections 3.2.

References

(1) "EIA Annual Energy review 2010," U.S. Energy Information Administration, October 2011, URL: http://www.eia.gov/totalenergy/data/annual/pdf/aer.pdf.

(2) "BP Statistical Review of World Energy, URL:http://www.bp.com/content/dam/bp/pdf/statistical-review/statistical_review_of_world_energy_2013.pdf," **2013**, 8, .

(3) Knothe, G. *Fuel Processing Technology* **2005**, *86*, 1059.

(4) Ramos, M. J.; Fernandez, C. M.; Casas, A.; Rodriguez, L.; Perez, A. *Bioresource Technology* **2009**, *100*, 261.

(5) Martin, M. A. *New Biotechnology* **2010**, *27*, 596.

(6) Serrano-Ruiz, J. C.; Dumesic, J. A. *Energy & Environmental Science* **2011**, *4*, 83.

(7) Regalbuto, J. *Computers & Chemical Engineering* **2010**, *34*, 1393.

(8) "Biomass as Feedstock for a Bioenergy and Bioproducts Industry: The Technical Feasibility of a Billion-Ton Annual Supply " U.S. Department of Energy, **2005**, URL: http://www1.eere.energy.gov/biomass/pdfs/final_billionton_vision_report2.pdf.

(9) Haag, A. L. *Nature* **2007**, *447*, 520.

(10) Luque, R. *Energy & Environmental Science* **2010**, *3*, 254.

(11) Subhadra, B. G. *Energy Policy* **2010**, *38*, 5892.

(12) Banerji, R.; Misra, G.; Nigam, S. K. *Journal of Scientific & Industrial Research* **1983**, *42*, 686.

(13) Demirbas, A. *Energy Sources Part B-Economics Planning and Policy* **2009**, *4*, 310.

(14) Kumar, A.; Sharma, S. *Renewable & Sustainable Energy Reviews* **2011**, *15*, 1791.

(15) Huber, G. W.; O'Connor, P.; Corma, A. *Applied Catalysis a-General* **2007**, *329*, 120.

(16) Donnis, B.; Egeberg, R. G.; Blom, P.; Knudsen, K. G. *Topics in Catalysis* **2009**, *52*, 229.

(17) Kubicka, D.; Simacek, P.; Zilkova, N. *Topics in Catalysis* **2009**, *52*, 161.

(18) Maki-Arvela, P.; Kubickova, I.; Snare, M.; Eranen, K.; Murzin, D. Y. *Energy & Fuels* **2007**, *21*, 30.

(19) Do, P. T.; Chiappero, M.; Lobban, L. L.; Resasco, D. E. *Catalysis Letters* **2009**, *130*, 9.

(20) Bertero, M.; de la Puente, G.; Sedran, U. *Fuel* **2012**, *95*, 263.

(21) Behtash, S.; Lu, J. M.; Faheem, M.; Heyden, A. *Green Chemistry* **2014**, *16*, 605.

(22) Lu, J. M.; Behtash, S.; Heyden, A. *Journal of Physical Chemistry C* **2012**, *116*, 14328.

(23) Xu, L. J.; Xu, Y. *Surface Science* **2010**, *604*, 887.

(24) Kresse, G.; Hafner, J. *Physical Review B* **1993**, *48*, 13115.

(25) Kresse, G.; Furthmuller, J. *Computational Materials Science* **1996**, *6*, 15.

(26) Kresse, G.; Hafner, J. *Physical Review B* **1993**, *47*, 558.

(27) Kresse, G.; Joubert, D. *Physical Review B* **1999**, *59*, 1758.

(28) Perdew, J. P.; Yue, W. *Physical Review B* **1986**, *33*, 8800.

(29) Perdew, J. P.; Wang, Y. *Physical Review B* **1992**, *45*, 13244.

(30) Perdew, J. P.; Burke, K.; Wang, Y. *Physical Review B* **1996**, *54*, 16533.

(31) Grimme, S. *Journal of Computational Chemistry* **2006**, *27*, 1787.

(32) Henkelman, G.; Uberuaga, B. P.; Jonsson, H. *Journal of Chemical Physics* **2000**, *113*, 9901.
(33) Henkelman, G.; Jonsson, H. *Journal of Chemical Physics* **1999**, *111*, 7010.
(34) Heyden, A.; Bell, A. T.; Keil, F. J. *Journal of Chemical Physics* **2005**, *123*.
(35) Truhlar, D. G.; Garrett, B. C.; Klippenstein, S. J. *Journal of Physical Chemistry* **1996**, *100*, 12771.
(36) Buzzi-Ferraris, G. *"BzzMath: Numerical libraries in C++", Politecnico di Milano:* www.chem.polimi.it/homes/gbuzzi.
(37) Pallassana, V.; Neurock, M. *Journal of Catalysis* **2002**, *209*, 289.
(38) Lu, J. M.; Behtash, S.; Faheem, M.; Heyden, A. *Journal of Catalysis* **2013**, *305*, 56.
(39) Simakova, I.; Rozmyslowicz, B.; Simakova, O.; Maki-Arvela, P.; Simakov, A.; Murzin, D. Y. *Topics in Catalysis* **2011**, *54*, 460.
(40) Lestari, S.; Maki-Arvela, P.; Simakova, I.; Beltramini, J.; Lu, G. Q. M.; Murzin, D. Y. *Catalysis Letters* **2009**, *130*, 48.
(41) Maki-Arvela, P.; Rozmyslowicz, B.; Lestari, S.; Simakova, O.; Eranen, K.; Salmi, T.; Murzin, D. Y. *Energy & Fuels* **2011**, *25*, 2815.
(42) Simakova, I.; Simakova, O.; Maki-Arvela, P.; Murzin, D. Y. *Catalysis Today* **2010**, *150*, 28.
(43) Lestari, S.; Maki-Arvela, P.; Eranen, K.; Beltramini, J.; Lu, G. Q. M.; Murzin, D. Y. *Catalysis Letters* **2010**, *134*, 250.
(44) Rozmyslowicz, B.; Maki-Arvela, P.; Tokarev, A.; Leino, A. R.; Eranen, K.; Murzin, D. Y. *Industrial & Engineering Chemistry Research* **2012**, *51*, 8922.
(45) Lugo-Jose, Y. K.; Monnier, J. R.; Williams, C. T. *Applied Catalysis a-General* **2014**, *469*, 410.
(46) Grabow, L. C.; Hovlbak, B.; Norskov, J. K. *Top. Catal.* **2010**, *53*, 298.
(47) Snare, M.; Kubickova, I.; Maki-Arvela, P.; Eranen, K.; Warna, J.; Murzin, D. Y. *Chemical Engineering Journal* **2007**, *134*, 29.
(48) Campbell, C. T. *Topics in Catalysis* **1994**, *1*, 353.
(49) Campbell, C. T. *Journal of Catalysis* **2001**, *204*, 520.
(50) Stegelmann, C.; Andreasen, A.; Campbell, C. T. *Journal of the American Chemical Society* **2009**, *131*, 8077.
(51) Kozuch, S.; Shaik, S. *Journal of the American Chemical Society* **2006**, *128*, 3355.